

Precision Position Measurement of Moving Atoms Using Optical Fields

K. D. Stokes, C. Schnurr, J. R. Gardner, M. Marable, G. R. Welch, and J. E. Thomas

Physics Department, Duke University, Durham, North Carolina 27706

(Received 19 June 1991)

We demonstrate optical techniques for precisely measuring the position of moving atoms. Micron spatial resolution is attained by the methods which ultimately will scale to yield nanometer resolution limited by the uncertainty principle.

PACS numbers: 42.50.Vk, 32.80.Pj

In this Letter we demonstrate new state-selective optical techniques for precisely measuring the position of moving atoms. The methods employ Raman-induced resonance imaging [1,2] in which a spatially varying potential correlates an atomic resonance frequency with the atomic position. Optical methods are ideally suited for high-resolution resonance imaging because they permit the study of very small volumes, which facilitates the application of large spatially varying potentials. Further, these optical techniques do not require mechanical surfaces (wires, slits, electrodes, etc.) to be placed in the region to be studied. In the first experiments, which are described below, a magnetic-field gradient provides a spatial variation of the resonance frequency yielding spatial resolution of $1.7 \mu\text{m}$. This is near the theoretical limit predicted for the transverse velocity spread for the atomic beam employed in the experiments. This demonstration paves the way for new experiments employing large spatially varying light shifts which are expected to achieve suboptical wavelength spatial resolution down to the nanometer region, limited by the uncertainty principle.

The development of these techniques has been motivated by the recent progress and interest in the creation of atomic spatial distributions which vary over small length scales. In atomic beams, such distributions arise by diffraction [3], periodic spatial modulation [4], channeling [5], focusing [6,7], and cooling [8]. In general, the distributions exhibit momentum-space coherence and are of both practical and fundamental interest. Recently, techniques have been developed for precise velocity selection [9] which are complementary to the techniques presented in this Letter. Many of these achievements have been spurred on, in part, by the advent of practical laser-cooling techniques [10]. Important applications include atomic interferometry, gyroscopes, and the creation of submicron structures by atomic deposition [3,4]. While techniques exist to create suboptical wavelength atomic spatial modulation and interference in atomic beams, methods for detection have been limited principally to hot wires or mechanical slits. Only in Ref. [5] is optical absorption used to determine an atomic position distribution. In that work, atoms are channeled in an off-resonant optical standing wave.

As discussed below and in Refs. [1,2], the fundamental limits on spatial resolution for the Raman-induced reso-

nance imaging method are determined by the interplay between maximizing spectral resolution and minimizing atomic motion along the measurement x axis, which is perpendicular to the atomic beam. In general, this atomic motion includes the velocity of the atoms along the measurement axis, acceleration imparted by the spatially varying potential, and wave mechanical diffraction. The best possible spatial resolution is achieved by choosing an optimum transit time across the optical field region. Transit-time-limited spectral resolution is easily achieved by using optically induced Raman transitions between long-lived states. The combination of optimum spectral resolution with a large spatially varying potential maximizes spatial resolution. As described below and in Ref. [2], appropriate configurations generally require that the size of the measurement region be quite small, which is readily accomplished using focused laser fields to induce the Raman transitions.

An important feature of the method is that the spatially varying potential affects only the final atomic state of a Raman transition, while the initial state is unaffected. This permits the initial state to propagate into the Raman region without perturbation. Assuming that the spatially varying potential varies linearly along the x axis only, the final atomic state energy is shifted according to

$$V(x) = -(x - x_0)F, \quad (1)$$

where F is just the classical force exerted on the final state by the spatially varying potential and x_0F is the shift from an adjustable, spatially constant field. The spatial resolution Δx is determined by the spectral resolution $\Delta\omega$ according to $\Delta V = F\Delta x = \hbar\Delta\omega$. With transit-time-limited resolution for the Raman transition, the spectral resolution is just $\Delta\omega = 1/T$, where T is the transit time across the Raman laser beams. Hence,

$$\Delta x = \hbar/FT. \quad (2)$$

Using Eq. (2), it is readily shown that the Raman-induced resonance imaging method can yield *uncertainty-principle-limited* spatial resolution for highly collimated atomic beams where the transverse momentum $Mv_x \ll FT$. An atom can make a transition from the initial state into the final state at any time during the transit time T . Since the force only is applied to the final state, an atom making a transition initially upon entering the

Raman laser beams acquires a transverse momentum FT , while an atom making the transition just before leaving the Raman beams acquires no transverse momentum. Thus, the momentum spread Δp due to the applied potential is FT . In this case, according to Eq. (2), atoms which make a transition to the final state emerge from the Raman region in a localized wave packet of width Δx and with a momentum spread Δp imparted by the spatially varying potential which obeys $\Delta x \Delta p = \hbar$. Under certain conditions, a minimum-uncertainty Gaussian wave packet can be produced [2].

With less collimation, the spatial resolution is limited by the transverse thermal velocity spread. In this case, the best possible velocity-limited spatial resolution, Δx_{vel} , can be understood physically as follows. By increasing the transit time T , the spectral resolution is increased. However, during the time T an atom of transverse velocity v_x will move along the x axis a distance $v_x T$. To achieve the optimum spatial resolution T must be limited to times of order $T = \Delta x_{\text{vel}}/v_x$. Using this as the maximum transit time in Eq. (2) yields $\Delta x_{\text{vel}} = (\hbar v_x/F)^{1/2}$. The corresponding diameter d of the Raman region for a supersonic beam of speed v_y is just $v_y T = \Delta x/\theta$, where θ is the beam collimation half angle.

A more careful calculation [2] yields velocity-limited resolution

$$\Delta x_{\text{vel}} = (2\hbar v_x/F)^{1/2}, \quad (3)$$

which differs from the heuristic result by $\sqrt{2}$. In this calculation, the Raman laser fields are assumed to have Gaussian intensity distributions and the optimum intensity $1/e$ width is found to be $d = \Delta x_{\text{vel}}/\theta$. For Gaussian laser fields, the fluorescence signal S , measured in the final-state detection region (see Figs. 1 and 2), can be shown to depend on the Wigner phase-space distribution for the initial atomic state, $\rho_i(v_x, x')$, according to

$$S(x_0) \propto \eta_R \int dv_x dx' R_1(x' - x_0, v_x) \rho_i(v_x, x'), \quad (4)$$

where R_1 is the spatial resolution function given by Eq. (19) of Ref. [2] and η_R is the Raman transition probability for $F=0$. For optimized velocity-spread-limited spatial resolution, R_1 takes the simple form

$$R_1(x' - x_0, v_x) = \frac{1}{\sqrt{2}} \exp \left[-\frac{(x' - x_0)^2}{\Delta x_{\text{vel}}^2} \right], \quad (5)$$

where it is assumed that the incident phase-space distribution is specified at the center of the Raman region. According to Eqs. (4) and (5), the spatial resolution given by Eq. (3) determines the $1/e$ width of a Gaussian spatial resolution function which is convoluted with the incident phase-space distribution.

We demonstrate the Raman-induced resonance imaging method in a samarium supersonic beam using the ${}^7F_1 \rightarrow {}^7F_0$ transition of ${}^{152}\text{Sm}$ at 570.65 nm, Fig. 1. Samarium was chosen for its convenient ground-state lev-

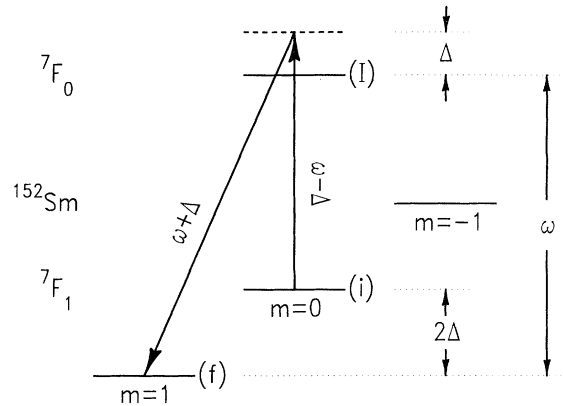


FIG. 1. Energy levels of ${}^{152}\text{Sm}$ used for Raman-induced resonance imaging. The laser frequency ω is locked to the $f \rightarrow I$ transition frequency. A uniform magnetic field splits levels i and f by $2\Delta \approx 220$ MHz.

el structure, absence of nuclear spin, and convenient optical resonance frequency. Atoms which are initially in the $m=0$ sublevel of the 7F_1 ground state make a Raman transition to the $m=+1$ sublevel via the 7F_0 excited state which serves as an off-resonant intermediate state. The $m=+1$ state, which is emptied prior to the Raman region by optical pumping, is detected after the Raman region by resonance fluorescence. A spatially varying magnetic field shifts the $m=+1$ state (g factor of 1.5), so that the resonance frequency of the Raman transition is dependent on the position of the incident atoms along the measurement x axis. Equations (4) and (5) assume that the difference frequency for the Raman fields is chosen to yield resonance at the point $x=x_0$. The point x_0 is readily shifted by tuning a uniform magnetic field. Detecting final-state fluorescence downstream from the Raman region versus uniform magnetic field determines the spatial distribution of atoms in the initial state with a resolution Δx_{vel} . Physically, the fluorescence intensity induced in the detection region from the $m=+1$ final state is proportional to the number of incident atoms in the $m=0$ state near the point on the x axis where the Raman fields are resonant with the local Raman transition frequency.

The experimental arrangement is shown in Fig. 2. The spatially varying magnetic field used in the experiments consists of a linearly varying field with a constant gradient of 500 G/cm, plus a 100-G uniform magnetic field oriented along the z axis which shifts the $m=+1$ state by approximately 220 MHz. The gradient magnetic field is generated with two parallel copper tubes separated by 6 mm and carrying 100 A each in the same direction. With the atomic beam axis defined as y , the magnetic-field gradients are $\partial B_z/\partial x = \partial B_x/\partial z = 500$ G/cm. Because of the strong uniform field along the z axis, the spatially varying level shift of the $m=+1$ state is dominated by the linear

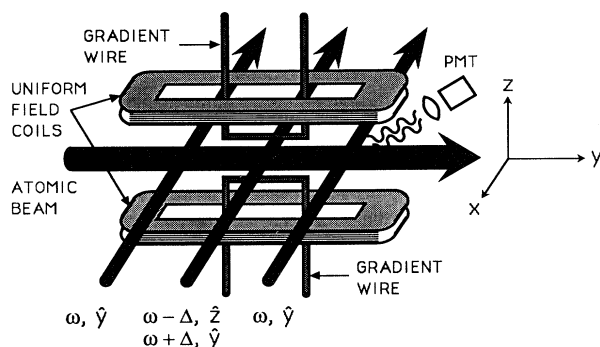


FIG. 2. Experimental arrangement. The gradient wires carry parallel currents. With the uniform field, this creates a shift of the f state which varies approximately linearly with position along the x axis. The f state is emptied by optical pumping by the first laser beam (ω). Atoms then enter the Raman region where the two overlapping laser beams ($\omega \pm \Delta$) cause transitions from state i to state f in a localized region along the x axis. Atoms which emerge in state f are detected by laser-induced fluorescence in the final region (ω).

variation of the z magnetic field along the x axis. This yields a linearly varying energy for the $m = +1$ state, and hence for the Raman transition, of 10^9 Hz/cm along the x axis.

The two copropagating optical fields which induce the Raman transition are derived using acousto-optic frequency shifting of ± 110 MHz from a single stable cw dye laser operating at 570.65 nm. These two beams are orthogonally polarized and combined in a single-mode polarization-preserving optical fiber to ensure good mode matching and parallel propagation of the Raman fields. The intensities of the off-resonant Raman fields are chosen so that the light shifts of the $m = 0$ and $m = +1$ states are equal. Since the Raman resonance condition requires only that the difference frequency of the optical fields match the splitting between the initial and final states, dye-laser frequency jitter and unwanted Doppler frequency shifts due to the finite atomic and laser beam collimation are eliminated. Additionally, the excited-state spontaneous decay rate does not enter into the linewidth of the Raman transition. Hence, transit-time-limited spectral resolution is obtained [11].

The optimum spatial resolution in the present experiments can be estimated from the previous discussion. Since V/h is the level shift of the final $m = +1$ state in Hz, in the present experiments $F/h = 10^9$ Hz/cm. The supersonic speed of the samarium beam is found by time-of-flight measurements to be $v_y = 9 \times 10^4$ cm/sec. For supersonic beams, the effective oven aperture due to collisions is larger than the actual oven aperture, making the collimation angle uncertain. The collimation half angle θ is estimated by measuring the Doppler width of a one photon transition after a 100- μ m slit placed 10 cm from the oven aperture. This yields $\theta \approx 0.5$ –1 mrad. For

$\theta = 1$ mrad, $v_x = 90$ cm/sec, and Eq. (3) determines the optimum spatial resolution $\Delta x \approx 1.7 \mu\text{m}$. The corresponding optimum diameter (FWHM) of each of the Raman fields is 2.8 mm. With the gradient magnetic field turned off, this corresponds to a Raman linewidth (FWHM) of 210 kHz as is readily shown from the weak-field Raman line shape for Gaussian laser beams in the transit-time limit. These values were used in our experiment.

Experimental measurements of the Raman line shape with the gradient magnetic field off are obtained by monitoring fluorescence in the detection region versus uniform magnetic field. The measured linewidth of 200 kHz (FWHM) is in nearly exact agreement with that expected in the transit-time limit. Although the theoretical analysis assumes weak Raman fields, in practice it is convenient to increase the Raman laser intensities to increase the transition probability. In the optimum case, the Raman "pulse area" ϕ in the atom frame should be approximately π . A strong-field theory of the Raman line shape for an off-resonant intermediate state (i.e., a two-level theory without decay) shows that no broadening of the line is expected provided that the ground-state light shifts induced by the Raman fields are equal and $\phi \approx \pi$. The measured line shape taken for $\phi = \pi$ confirms this result. Hence, in the position measurements, the Raman field intensities are left at the optimized levels.

For high spatial resolution with the gradient magnet on, the Raman laser beams must be focused and precisely centered along the vertical z axis between the two gradient magnet wires. This is due to the $\partial B_x / \partial z$ contribution to the $m = +1$ level shift which leads to a position smearing in our experiment given by $2.5 \text{ cm}^{-1} \langle z^2 \rangle$. The vertical FWHM of the Raman beams is therefore focused to $\approx 75 \mu\text{m}$, which reduces the smearing below $0.4 \mu\text{m}$. Precise centering is accomplished spectroscopically, by reversing the current in one of the parallel wires of the gradient magnet. In this case, the Raman linewidth with the gradient on can be shown to narrow dramatically when the Raman beams are precisely centered with respect to the gradient wires compared to when they are not centered.

For this experiment, a 25- μ m-diam gold-coated tungsten wire is placed at the center of the Raman fields, perpendicular to and at the center of the atomic beam. The shadow which is cast in the atomic beam is measured to demonstrate the method. The Raman-induced resonance image of the wire is shown in Fig. 3. The known wire diameter confirms the gradient magnet calibration and the steepness of the rising edge of the fluorescence signal versus uniform field determines the experimental position resolution $\Delta x = 1.7 \mu\text{m}$. This is consistent with the prediction of the optimum resolution, Eq. (3), for a collimation half angle somewhat less than 1 mrad, and $0.4 \mu\text{m}$ of $\langle z^2 \rangle$ -dependent position smearing.

In conclusion, we have demonstrated a Raman-induced

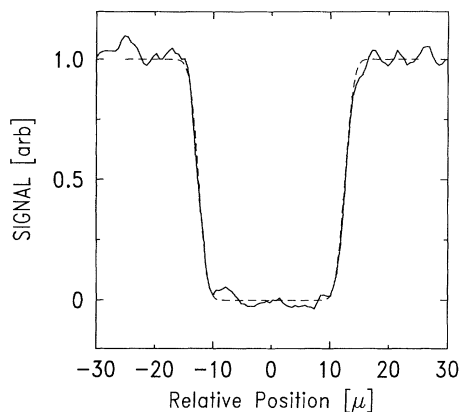


FIG. 3. Raman-induced resonance image of the shadow cast in the atomic beam by a 25- μm wire. The solid line is the data. The dashed line is the theoretical prediction for a spatial resolution of 1.7 μm . The signal is the fluorescence intensity in the final region vs uniform magnetic field.

resonance imaging technique which is capable of high spatial resolution and which provides a general state-selective method for the position measurement and localization of moving atoms. Experiments in progress will utilize spatially varying light shifts to create and study suboptical wavelength scale one-dimensional atomic wave packets. Scaling to higher resolution is limited by the signal-to-noise ratio because fewer atoms are sampled. However, using single-atom detection for the final state ultimately will permit scaling to nanometer spatial resolution limited by atomic diffraction and acceleration [2].

Many new applications of the Raman-induced resonance imaging method are readily envisioned. Since the spatially varying potential affects only the final state of the Raman transition, this technique can be used to determine the initial-state spatial distribution arising in a wide variety of experiments. These include atomic interferometry [12], studies of localized atoms in cavities and

near surfaces [13], generation of position squeezed states in harmonic wells [14], measurements of trapped-atom spatial distributions using pulsed Raman fields, and atomic two-point spatial correlation. Further, novel atomic optics can be developed based on high-resolution position-dependent depletion of the incident beam.

This work is supported by RADC Contract No. F19628-88-K-0012, ARO Grant No. DAAL03-90-G-0114, and NIST Grant No. 60NANB0D1053.

-
- [1] J. E. Thomas, *Opt. Lett.* **14**, 1186 (1989).
 - [2] J. E. Thomas, *Phys. Rev. A* **42**, 5652 (1990).
 - [3] P. E. Martin, B. G. Oldaker, A. H. Miklich, and D. E. Pritchard, *Phys. Rev. Lett.* **60**, 515 (1988).
 - [4] V. P. Chebotayev, B. Ya. Dubetsky, A. P. Kasantsev, and V. P. Yakovlev, *J. Opt. Soc. Am. B* **2**, 1791 (1985).
 - [5] C. Salomon, J. Dalibard, A. Aspect, H. Metcalf, and C. Cohen-Tannoudji, *Phys. Rev. Lett.* **59**, 1659 (1987).
 - [6] V. I. Balykin and V. S. Letokhov, *Phys. Today* **42**, No. 4, 23 (1989).
 - [7] N. Bigelow and M. G. Prentiss, in *Technical Digest Series* (Optical Society of America, Washington, DC, 1990), Vol. 15, p. 238.
 - [8] A. Aspect, E. Arimondo, R. Kaiser, N. Vansteenkiste, and C. Cohen-Tannoudji, *Phys. Rev. Lett.* **61**, 826 (1988).
 - [9] M. Kasevich, D. S. Weiss, E. Riis, K. Moler, S. Kasapi, and S. Chu, *Phys. Rev. Lett.* **66**, 2297 (1991).
 - [10] See, for example, W. D. Phillips, J. V. Prodan, and H. J. Metcalf, *J. Opt. Soc. Am. B* **2**, 1751 (1985).
 - [11] J. E. Thomas, P. R. Hemmer, S. Ezekiel, C. C. Leiby, Jr., R. H. Picard, and C. R. Willis, *Phys. Rev. Lett.* **48**, 867 (1982).
 - [12] O. Carnal and J. Mlynek, *Phys. Rev. Lett.* **66**, 2689 (1991); D. W. Keith, C. R. Ekstrom, Q. A. Turchette, and D. E. Pritchard, *Phys. Rev. Lett.* **66**, 2693 (1991).
 - [13] A. Anderson, S. Haroche, E. Hinds, W. Jhe, and D. Meshede, *Phys. Rev. A* **37**, 3594 (1988).
 - [14] H. P. Yuen, *Phys. Rev. Lett.* **51**, 719 (1983).